Supplementary Materials: Stability of Hydroxo/Oxo/Fluoro Zirconates vs. Hafniates — A DFT Study

Jennifer Anders[1] *⬛, Fabian Göritz[1], Anselm Loges[2], Timm John[2], Beate Paulus[1]

Contents

1. Literature Overview

Table S1. Literature overview on calculated bulk MO$_2$ and MF$_4$ monoclinic crystals with M = Zr or Hf. For plain wave calculations the cutoff energy is given in eV. The *k*-grid is given as k_axk_bxk_c or if not available in number of irreducible *k*-points ($k_{irred.}$). The main aims are abbreviated as phase transitions (PT), band structure or gap (BS), elastic (EP) and dielectric properties (DP) or phonon spectra (Ph):

	system	setup	aim
Králik et al.[1]	ZrO$_2$	LDA+GW(-/1361 eV/2 $k_{irred.}$)	BS
Jomard et al. [2]	ZrO$_2$	LDA+PW91+PB(VASP/300 eV/4x4x4)	PT
Kuwabara et al. [3]	ZrO$_2$	PW91(VASP/500 eV/3x3x3)	PT
Fadda et al.[4,5]	ZrO$_2$	LDA+PBE(ABINIT/1633 eV/4x4x4)	EP+DP+Ph
Delarmelina et al.[6]	ZrO$_2$	PBE+PBEsol+RPBE+TPSS w/o +U w/o D2/D3(VASP/550 eV/5x5x5)	PT+BS+EP+DP
Demkov[7]	ZrO$_2$+HfO$_2$	LDA(CASTEP/750 eV/4x4x4)	BS
Zhao and Vanderbilt[8,9]	ZrO$_2$+HfO$_2$	LDA+PBE(-/340 eV/4x4x4)	Ph+DP
Jaffe et al.[10]	ZrO$_2$+HfO$_2$	LDA+PW91(VASP/495 eV/9x9x9)	PT+BS
Luo et al.[11]	ZrO$_2$+HfO$_2$	LDA(VASP/800 eV/8x8x8)	PS+Ph
Mullins et al.[12]	ZrO$_2$+HfO$_2$	PBE(VASP/550 eV/6x6x6)	surface etching
Debernardi and Fanciulli[13]	HfO$_2$	LDA(PWSCF/476 eV/4x4x4)	PT+Ph
Li et al.[14]	HfO$_2$	LDA+8eV Hf-5d +6eV O-2p (CASTEP/380 eV/24x24x24)	BS
Li et al.[15]	HfO$_2$	LDA+8eV Hf-5d +4.35 eV O-2p (CASTEP/380 eV/6x6x6)	BS
Laudadio et al.[16]	HfO$_2$	PBE+6eV Hf-5d +4eV O-2p (QuantumATK/1200 eV/15x15x15)	
Low et al.[17]	HfO$_2$	PBEsol(ABINIT/2721 eV/6x6x6)	PT+Ph
Rivas-Silva et al. [18]	ZrF$_4$+HfF$_4$	CIS(Gaussian/STO/cluster)	BS

2. Choice of Functional

Delarmelina et al.[6] published a very elaborate benchmark on various properties for the three phases of ZrO$_2$ with different functionals (PBE, PBEsol, RPBE and TPSS) with/without D2 or D3 dispersion correction and/or Hubbard-type correction (+U) onto Zr-4d. For the performance onto the atomic structure of monoclinic ZrO$_2$, they found that the relative error versus experiment for each lattice vector varies just from 0.2–0.3% (PBEsol) to 1.2–2.2% (RPBE). For the original PBE, the relative errors are in between with 0.7–1.2%.

Thus, there is little variation between these meta-/GGA functionals onto the very ionic bulk crystal. When comparing the +U correction, the relative lattice vector errors even grow with U. At the highest U = 8 eV, these are 1.7–3.3% (PBEsol+U 8 eV) to 2.9–4.9% (RPBE+U 8 eV). By applying D3 on a smaller U of 2 eV, the relative errors are considerably lower again with 0.1–0.6% (PBEsol+U 2 eV + D3) to 1.5–1.6% (RPBE+U 2 eV +D3), but still higher than PBEsol without any addition. It should also be noted that Delarmelina et. al. refer their results to an older experimental value with lattice vectors of $a = 5.145$ Å, $b = 5.207$ Å and $c = 5.242$ Å [19]. When instead referencing to the slightly larger values of $a = 5.150$ Å, $b = 5.212$ Å and $c = 5.317$ Å measured 23 years later by high-resolution neutron powder diffraction [20], the relative errors of their reported PBE (550 eV cutoff/5x5x5 k-grid) are significantly smaller with 0.2–0.8%. Compared to this newer experimental value, their tested 0.1–1.8% (PBEsol+U 2 eV + D3) performs equally in relative errors as simple PBEsol but worse than simple PBE. By using the hard PAW-potential on oxygen, the accurate numerical setting and a larger cutoff, our now reported PBE (773 eV cutoff/4x4x4 k-grid) vectors are even closer with only 0.1–0.3%. Summing up, on geometrical data of monoclinic ZrO_2, applying a dispersion correction or +U correction onto the Zr-4d does not improve the results.

The reason behind the non-observed enhancement by +U onto the crystal structure lies within the nominal IV oxidation state, which is present in all the studied bulk crystals within this paper. Formally, Zr(IV) possesses the electronic configuration of krypton and Hf(IV) of xenon. Measurements on MO_2 have shown, that the Zr(IV)-4d and Hf(IV)-5d form the conduction band (CB) instead of the valence band (VB), which is constructed from the O-2p suggesting that there are no correlated d-electrons to localize by +U [21,22]. For a longer discussion we would also like to refer to a study on HfO_2 by Low et al. [17].

We have seen that other authors use LDA+U on MO_2 with a big +U of 8 eV on Zr-4d (or 6–8 eV on Hf-5d), in combination with another 4.35 eV (or 4-6 eV for HfO_2) on O-2p to obtain better band gap agreement [14–16]. However, for the reasons above, we chose to not apply a large +U onto non-occupied orbitals and to simultaneously apply two empirical +U parameters on a binary compound.

Moreover, we do not expect that the Zr-4d and Hf-5d CB significantly mixes into the bonding to oxide or fluoride, as the band gaps of these materials are far in the insulating regime (ZrO_2: 5.83 eV [21]; HfO_2: 5.86 eV [23]; ZrF_4: 9.4 eV [18]; HfF_4: 10.3 eV [18]). It is well known, that GGAs generally underestimate band gaps as the electronic structure is too delocalized. However, given the high band gaps of these ionic crystals, there is a large tolerance before the underestimation would severely change the nature of conductivity. As our paper does not discuss band structures, electronic excitations or other optical properties but merely relative stabilities between the bulk solids, we chose the simple GGA approach.

3. Convergence of Computational Setup

Unless stated differently, the computational details given in the main paper apply.

3.1. k-grid Convergence

The k-grid has been tested for convergence by single point calculations on the respective experimental crystal structures. All grids are Monkhorst-Pack-type and possess an equal number of k-points in all three dimensions. For the metallic unit cells, the converged smearing width of 0.05 eV has been applied. As the metallic unit cells are just needed for the cohesive energies with elemental reactants (see main paper Table 2), we considered the convergence of $\Delta E_0 \leq 2.5$ meV per unit cell enough and chose to not increase the k-grid further than $n = 17$.
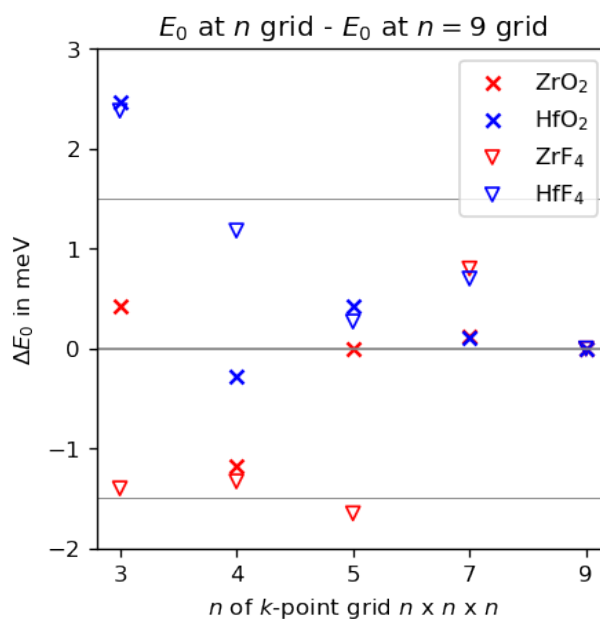
Figure S1. k-grid convergence for ionic unit cells. Plotted is the difference in total energy in meV per unit cell to the finest grid (ΔE_0). The convergence area of $\Delta E_0 \leq 1.5$ meV is visualized by two horizontal lines. Values for $n = 1, 2$ are not included in this zoomed-in plot due to their high deviation.

Table S2. k-grid converged total energies (E_0) in eV for ionic unit cells. Given are the values for the finest grid, the within 1.5 meV converged grid size and their difference (ΔE_0). The latter is also plotted in Figure S1:

compound	E_0 ($n = 4$)	E_0 ($n = 9$)	ΔE_0
ZrO_2	-115.13051	-115.12933	-118×10^{-5}
HfO_2	-133.12904	-133.12876	-28×10^{-5}
ZrF_4	-205.28538	-205.28405	-133×10^{-5}
HfF_4	-232.20100	-232.20218	118×10^{-5}
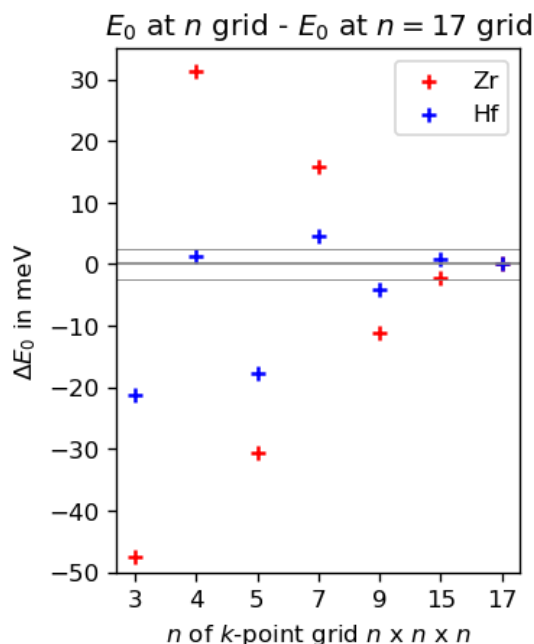
Figure S2. k-grid convergence for metallic unit cells. Plotted is the difference in total energy in meV per unit cell to the finest grid (ΔE_0). The convergence area of $\Delta E_0 \leq 2.5$ meV is visualized by two horizontal lines. Values for $n = 1, 2$ are not included in this zoomed-in plot due to their high deviation.

Table S3. k-grid converged total energies (E_0) in eV for metallic unit cells. Given are the values for the finest grid, the within 2.5 meV converged grid size and their difference (ΔE_0). The latter is also plotted in Figure S2:

compound	E_0 ($n = 15$)	E_0 ($n = 17$)	ΔE_0
Zr	-17.042727	-17.040550	-218×10^{-5}
Hf	-25.479629	-25.480518	89×10^{-5}

3.2. Electronic Smearing Convergence

For the two metallic unit cells of Zr and Hf, the second order Methfessel-Paxton smearing has been tested for different smearing widths (σ) by single point calculations on the respective experimental crystal structures applying the converged k-grid of $n = 15$. The σ-value of 0.05 eV has been selected for both metals as it yields the smallest deviation between total energy (E_0) and free energy at 0 K (F), which differ by the electronic entropy. However, for the set of tested values, all give a much smaller deviation than the k-grid convergence error. Therefore, as well as we only need the total energy of the metal unit cell to construct the cohesion energies, we did not sample further σ-values.
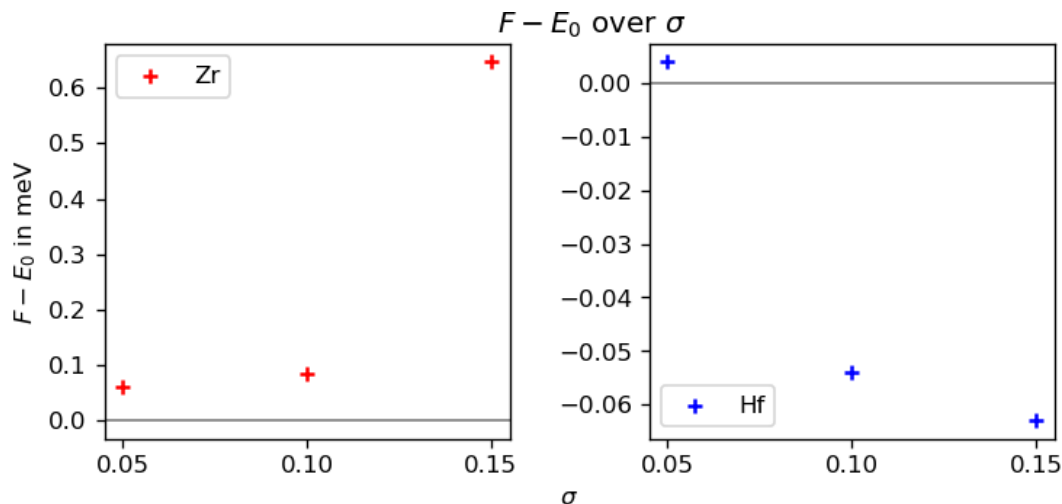
Figure S3. Second order Methfessel-Paxton smearing convergence for different smearing widths (σ) in meV per unit cell. Plotted is the difference of free energy at $0\,\mathrm{K}$ (F) minus the total energy (E_0).

4. Validation on Known Crystal Structures

4.1. Unit Cells of Known Crystals

To evaluate the performance of our computational setup on the geometrical parameters, Table S4 gives the calculated and literature unit cell parameters for all experimentally known crystal structures used within the main paper. It also gives the absolute difference to the experimental literature value (Δ exp) and the deviation from experiment in percentage ($\Delta_\%$ exp) according to Equation 1.

$$\Delta_\%\mathrm{exp} = \frac{|\mathrm{calc} - \mathrm{exp}|}{\mathrm{exp}} \times 100\% = \frac{\Delta\mathrm{exp}}{\mathrm{exp}} \times 100\% \tag{1}$$

Table S4. Relaxed unit cell parameters versus experimental (lit. exp) and calculated literature (lit. PB91) values. Given are the unit cell vector lengths (a, b, c), unit cell volume (V), unit cell volume per formula unit ($V_{\text{f.u.}}$) and the non-orthogonal angle (β), each relaxed parameter is also given as absolute difference to the experimental literature value (Δ exp) and the deviation from experiment in percentage ($\Delta_{\%}$ exp); note, that for monoclinic oxides and fluorides: $\alpha = \gamma = 90°$, while for hcp metals: $\alpha = \beta = 90°$ and $\gamma = 120°$:

Compound	a (Å)	b (Å)	c (Å)	V (Å³)	β (°)
ZrO$_2$	5.154	5.224	5.332	141.56	99.55
lit. PB91 [10]	5.197	5.279	5.349	144.74	99.53
lit. exp [20]	5.150	5.212	5.317	140.88	99.23
Δ exp	0.004	0.012	0.015	0.68	0.32
$\Delta\%$ exp	0.1	0.2	0.3	0.5	0.3
HfO$_2$	5.105	5.182	5.277	137.64	99.54
lit. PB91 [10]	5.128	5.191	5.297	139.25	99.71
lit. exp [24]	5.114	5.168	5.290	138.03	99.21
Δ exp	0.009	0.014	0.013	0.39	0.33
$\Delta\%$ exp	0.2	0.3	0.2	2.9	0.3
ZrF$_4$	11.694	9.889	7.660	710.40	126.68
lit. exp [25]	11.845	9.930	7.730	732.53	126.32
Δ exp	0.151	0.041	0.070	22.13	0.36
$\Delta\%$ exp	1.3	0.4	0.9	3.0	0.3
HfF$_4$	11.609	9.816	7.600	694.85	126.65
lit. exp [26]	11.725	9.869	7.636	713.48	126.15
Δ exp	0.116	0.053	0.036	18.63	0.50
$\Delta\%$ exp	1.0	0.5	0.5	2.6	0.4
Zr	3.234	3.234	5.168	46.82	
lit. exp. [27]	3.242	3.242	5.166	47.03	
Δ exp	0.008	0.008	0.002	0.21	
$\Delta\%$ exp	0.2	0.2	0.03	0.4	
Hf	3.202	3.202	5.056	44.91	
lit. exp. [28]	3.198	3.198	5.061	44.83	
Δ exp	0.004	0.004	0.005	0.08	
$\Delta\%$ exp	0.1	0.1	0.1	0.2	

4.2. Bonding Situation in Known Crystals

We also tested our computational method on the bond lengths published for the Zr-species. The bonding situation within the oxides is shown in Figure S4. The bond lengths between the metal center and each of the seven oxygen atoms are listed in Table S5. For any of the seven bond lengths, the difference to experiment $\left(\Delta R_{\text{Zr}-\text{O}}^{\text{exp}}\right)$ is only 0.000–0.011 Å. By that, $\Delta R_{\text{Zr}-\text{O}}^{\text{exp}}$ is one order of magnitude smaller than the difference between the two relaxed geochemical twins $\Delta R_{\text{M}-\text{O}}$, with one exception. For M$-$O$_4$, $\Delta R_{\text{M}-\text{O}_4}$ and $\Delta R_{\text{Zr}-\text{O}_4}^{\text{exp}}$ possess the same order of magnitude.
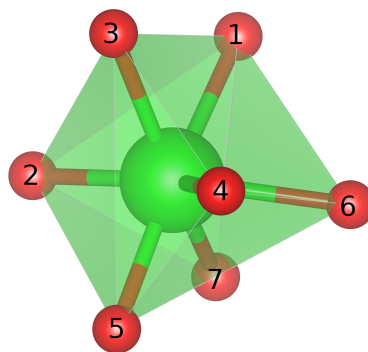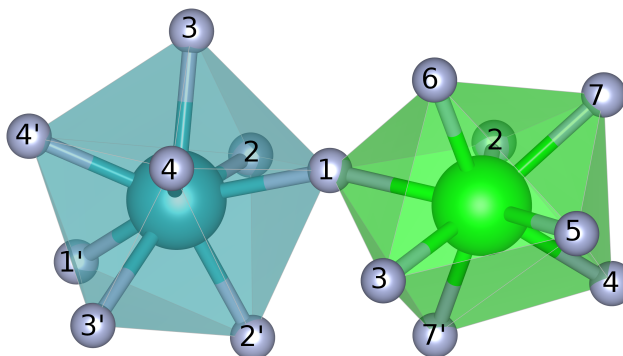
Figure S4. Bonding situation in a subunit of Zr/HfO_2. The oxygen atoms are labeled in accordance to the bond lengths given in Table S5.

Table S5. Bond lengths between metal center and oxygen atoms (R_{M-O}) in relaxed ZrO_2/HfO_2 with the absolute difference in bond length between the two M-species (ΔR_{M-O}). For comparison, also the experimental bond lengths for ZrO_2 $\left(R_{Zr-O}^{exp} \right)$ [20] are given together with the absolute difference to the relaxed values $\left(\Delta R_{Zr-O}^{exp} \right)$. All values are given in Å.

bond	R_{Zr-O}	R_{Hf-O}	ΔR_{M-O}	R_{Zr-O}^{exp} [20]	ΔR_{Zr-O}^{exp}
$M - O_1$	2.265	2.228	0.037	2.267	0.002
$M - O_2$	2.070	2.051	0.019	2.063	0.007
$M - O_3$	2.155	2.138	0.017	2.153	0.002
$M - O_4$	2.253	2.236	0.017	2.242	0.011
$M - O_5$	2.052	2.041	0.011	2.052	0.000
$M - O_6$	2.175	2.165	0.010	2.176	0.001
$M - O_7$	2.163	2.137	0.026	2.157	0.006

Figure S5. Bonding situation in a subunit of Zr/HfF_4. The fluorine atoms are labeled in accordance to the bond length in Table S6.

The bonding situation of the fluorides is shown in Figure S6 and listed in Table S6. In contrast to the oxides, the relaxed bond lengths differ stronger to the experimental bond lengths with 0.003–0.049 Å. Thus, ΔR_{Zr-F}^{exp} and ΔR_{M-F} are about the same order of magnitude for most bonds.

Table S6. Bond lengths between metal center and fluorine atoms (R_{M-F}) in relaxed ZrF_4/HfF_4 with the absolute difference in bond length between the two M-species (ΔR_{M-F}). For comparison, also the experimental bond lengths for ZrF_4 $\left(R_{Zr-F}^{exp}\right)$ [25] are given together with the absolute difference to the relaxed values $\left(\Delta R_{Zr-F}^{exp}\right)$. All values are given in Å.

bond	R_{Zr-F}	R_{Hf-F}	ΔR_{M-F}	R_{Zr-F}^{exp} [25]	ΔR_{Zr-F}^{exp}
$M_A - F_1$	2.082	2.067	0.015	2.072	0.010
$M_A - F_1'$	2.082	2.067	0.015	2.072	0.010
$M_A - F_2$	2.082	2.068	0.014	2.072	0.010
$M_A - F_2'$	2.082	2.068	0.014	2.072	0.010
$M_A - F_3$	2.151	2.133	0.018	2.180	0.029
$M_A - F_3'$	2.151	2.133	0.018	2.180	0.029
$M_A - F_4$	2.069	2.054	0.015	2.052	0.017
$M_A - F_4'$	2.069	2.054	0.015	2.052	0.017
$M_B - F_1$	2.097	2.033	0.064	2.132	0.035
$M_B - F_2$	2.110	2.093	0.017	2.159	0.049
$M_B - F_3$	2.096	2.083	0.013	2.127	0.031
$M_B - F_4$	2.085	2.068	0.017	2.088	0.003
$M_B - F_5$	2.126	2.111	0.015	2.148	0.022
$M_B - F_6$	2.051	2.035	0.016	2.048	0.003
$M_B - F_7$	2.095	2.076	0.019	2.118	0.023
$M_B - F_7'$	2.047	2.083	0.036	2.031	0.016

5. Literature ZPE Energies on MO_2

Table S7. ZPE energies per formula unit (f.u.) obtained from the published optical phonon frequencies at the Γ-point calculated with the PBE, LDA or PW91 functional:

		ZPE(MO_2) in eV/f.u.	
		M = Zr	M = Hf
Zhao and Vanderbilt[8]	PBE	—	0.190
Luo et al.[11]	LDA	0.203	0.206
Kuwabara et al. [3]	PW91	0.192	—
Fadda et al.[5]	LDA	0.202	—
	PBE	0.190	—

6. Discussion on Zr/Hf differences in ΔE vs. ΔG

The main focus of our paper is to compare the affinity of Zr(IV) vs. Hf(IV) to form oxide or fluorides. We do not strive to accurately predict the formation energy released under experimental conditions, but rather the relative energy difference between Zr and Hf. For the comparison of the respective Zr(IV) and Hf(IV) reaction in Table 2, only the solid bulk compound changes. The molecular reactants or products remain identical when comparing the same reaction. Within this study, we compare Zr(IV) and Hf(IV) bulk materials. Within the bulk crystals itself, we do expect little temperature and due to their hardness very little pressure dependent contributions. A pressure induced phase transition would only occur at 3 GPa for ZrO_2[29] and even 11 GPa for HfO_2[30]. Thermally, all studied Zr and Hf oxides and fluorides are stable until at least 910°C [29,31,32]. Ab initio molecular dynamics calculations on the monoclinic to tetragonal phase transition of HfO_2 found a linear temperature dependence of ΔG up to 730°C [17]. This suggests that the anharmonic contributions are only decisive for temperatures beyond. Within their surface etching study, Mullins et al.[12] did calculate their ΔG as:

$$\Delta G = \Delta E_{DFT} + \Delta ZPE + \Delta W(T) - T\Delta S + RT\ln(Q)$$

The last term of volume work ($RT\ln(Q)$) is included, as they considered a variable number of gaseous molecules and thus variable pressures for reactants and products. Most

importantly, they considered a bulk or surface to gas-phase reaction. Q is the quotient of partial pressures of gaseous products divided by gaseous reactants. As entropic contributions (ΔS), they included the translational entropy of the gaseous molecules, as well as the surface entropy. Both do not play a role when comparing the Zr vs. Hf difference in bulk to bulk reactions. The enthalpic contributions ($\Delta W(T)$) and the difference in zero point energy (ΔZPE) have been calculated for the gaseous molecules by the rigid rotator, harmonic oscillator model, as well as for the first layer of surface atoms by a harmonic phonon calculation. They do not clarify, whether they also performed a phonon calculation for the bulk compounds.

Table S7 lists all found harmonic phonon DFT calculations by literature. No phonon calculations could be found for the fluorides. The only found measured spectra could only resolve 20 vibrations for ZrF_4 but 29 for HfO_2, while by symmetry the monoclinic unit cell should have 27 optical phonons [33]. The ZPE of ZrO_2 at the LDA-level from Luo et al.[11] and Fadda et al.[5] agree very well, just do the two GGAs PBE and PW91 on ZrO_2. One also sees that the ZPE at the PBE-level is identical to at least 1 meV per formula unit between ZrO_2 and HfO_2 when comparing from two sources. The only source calculating the full phonon spectra of both compounds at the LDA-level of Luo et al.[11] gives a slightly higher ZPE for the heavier HfO_2 by 3 meV per formula unit.

Harmonic vibrations are proportional to the force constant and anti-proportional to the square root of the reduced mass. Judged by the mass, the vibrational frequencies of HfO_2 should be lower than for the much lighter ZrO_2. However, the Hf−O bond distances and thus the force constants of HfO_2 are significantly stronger. Because the mass difference dominates, the low frequency modes are considerably higher in energy for ZrO_2 than for HfO_2 as shown by calculations of Luo et al.[11] and measurements by Quintard et al. [34]. Within the high frequency regime of oxygen-dominated vibrations, both found slightly higher frequencies for HfO_2 than for ZrO_2 due to the stronger force constants.

Based on these observations on MO_2, we make the following assumptions for the ZPE of MF_4. Because of the slightly higher mass of F than O, the reduced masses of a single Hf−F bond grows stronger than the Zr one compared to the oxides. This should decrease the vibrational frequencies and thus lower the ZPE of HfF_4 vs. ZrF_4. Comparing the ZPE per formula unit of the oxides vs. the fluorides, we expect a considerably higher value for the latter, because the formula unit contains 5 instead of 3 atoms. However, all additional atoms are fluorine and all Hf−F bonds are also shorter and thus expected to have stronger force constant than Zr−F. Consequently, these should add more high frequency vibrations dominated by fluorine. These could make the possible difference between Hf and Zr-species even smaller than the found 0–3 meV per formula unit for the oxides. Summing up, we expect the effect of stronger mass increase per single M−F bond within the fluorides on the one side and more anion-dominated vibrations with shorter interatomic distance Hf−F than Zr−F on the other side to counterbalance as they did in the oxides.

6.1. Test Calculations in the Gas-Phase

To invest why the bulk to gas-phase reactions reported by Mullins et al. [12] predict the opposite Zr to Hf trend as our bulk to bulk reactions, we performed additional gas-phase calculations.

We relaxed tetrahedral ZrF_4 and HfF_4 in the gas-phase by ORCA 5.0.3[35] at the PBE/def2-TZVP[36] level applying D_2 symmetry, a TightSCF and a final DFT grid of 5. When applying the Karlsruhe basis of def or def2, most programs use the corresponding Stuttgart effective core potentials (ECP) per default. For Zr, this default ECP contains 28 core electrons, while for Hf, this default ECP is a very large core with 60 electrons [37]. For comparison, we performed the same relaxation as all-electron calculation with additional ZORA [38,39] to account for the scalar relativistic effects. By the analytical Hessian, we obtain the ZPE. The relaxed bond lengths and ZPE are given in Table S8.

Table S8. Comparison of M−F bond length in Å and ZPE in meV per formula unit for molecular ZrF_4 and HfF_4 with or without ZORA:

	PBE/def2-TZVP		PBE/def2-TZVP/ZORA	
	R_{M-F}	ZPE	R_{M-F}	ZPE
ZrF_4	1.103	217.5	1.100	214.3
HfF_4	1.104	209.7	1.097	214.3

Table S8 shows that with the default ECP, PBE predicts a too large Hf−F bond distance, which results in a too small ZPE. Note that this is not observed in the solid state calculations, that are giving a smaller Hf−F than Zr−F distance. These test calculations suggest that for the gas-phase, it is vital not to use the default large core on Hf but to include all electrons and treat the scalar relativistic effects more explicitly than by ECP. However, according to their paper, Mullins et al. [12] did not include any relativistic correlation. They also do not state if they used a non-default smaller core on Hf.

References

1. Králik, B.; Chang, E.K.; Louie, S.G. Structural properties and quasiparticle band structure of zirconia. *Phys. Rev. B* **1998**, *57*, 7027–7036. https://doi.org/10.1103/PhysRevB.57.7027.
2. Jomard, G.; Petit, T.; Pasturel, A.; Magaud, L.; Kresse, G.; Hafner, J. First-principles calculations to describe zirconia pseudopolymorphs. *Phys. Rev. B* **1999**, *59*, 4044–4052. https://doi.org/10.1103/PhysRevB.59.4044.
3. Kuwabara, A.; Tohei, T.; Yamamoto, T.; Tanaka, I. Ab initio lattice dynamics and phase transformations of ZrO_2. *Phys. Rev. B* **2005**, *71*, 64301. https://doi.org/10.1103/PhysRevB.71.064301.
4. Fadda, G.; Colombo, L.; Zanzotto, G. First-principles study of the structural and elastic properties of zirconia. *Phys. Rev. B* **2009**, *79*, 214102. https://doi.org/10.1103/PhysRevB.79.214102.
5. Fadda, G.; Zanzotto, G.; Colombo, L. First-principles study of the effect of pressure on the five zirconia polymorphs. II. Static dielectric properties and Raman spectra. *Phys. Rev. B* **2010**, *82*, 64106. https://doi.org/10.1103/PhysRevB.82.064106.
6. Delarmelina, M.; Quesne, M.G.; Catlow, C.R.A. Modelling the bulk properties of ambient pressure polymorphs of zirconia. *Phys. Chem. Chem. Phys.* **2020**, *22*, 6660–6676. https://doi.org/10.1039/D0CP00032A.
7. Demkov, A.A. Investigating Alternative Gate Dielectrics: A Theoretical Approach. *Phys. Status Solidi B* **2001**, *226*, 57–67. https://doi.org/10.1002/1521-3951(200107)226:1<57::AID-PSSB57>3.0.CO;2-L.
8. Zhao, X.; Vanderbilt, D. Phonons and lattice dielectric properties of zirconia. *Phys. Rev. B* **2002**, *65*, 75105. https://doi.org/10.1103/PhysRevB.65.075105.
9. Zhao, X.; Vanderbilt, D. First-principles study of structural, vibrational, and lattice dielectric properties of hafnium oxide. *Phys. Rev. B* **2002**, *65*, 233106. https://doi.org/10.1103/PhysRevB.65.233106.
10. Jaffe, J.E.; Bachorz, R.A.; Gutowski, M. Low-temperature polymorphs of ZrO_2 and HfO_2: A density-functional theory study. *Phys. Rev. B* **2005**, *72*, 144107. https://doi.org/10.1103/PhysRevB.72.144107.
11. Luo, X.; Zhou, W.; Ushakov, S.V.; Navrotsky, A.; Demkov, A.A. Monoclinic to tetragonal transformations in hafnia and zirconia: A combined calorimetric and density functional study. *Phys. Rev. B* **2009**, *80*, 134119. https://doi.org/10.1103/PhysRevB.80.134119.
12. Mullins, R.; Kondati Natarajan, S.; Elliott, S.D.; Nolan, M. Self-Limiting Temperature Window for Thermal Atomic Layer Etching of HfO_2 and ZrO_2 Based on the Atomic-Scale Mechanism. *Chem. Mater.* **2020**, *32*, 3414–3426. https://doi.org/10.1021/acs.chemmater.9b05021.
13. Debernardi, A.; Fanciulli, M. Structural and vibrational properties of high-dielectric oxides, HfO_2 and TiO_2: A comparative study. *Mater. Sci. Semicond. Process.* **2006**, *9*, 1014–1019. https://doi.org/10.1016/j.mssp.2006.10.036.
14. Li, J.; Han, J.; Meng, S.; Lu, H.; Tohyama, T. Optical properties of monoclinic HfO_2 studied by first-principles local density approximation + U approach. *Appl. Phys. Lett.* **2013**, *103*, 071916. https://doi.org/10.1063/1.4818765.
15. Li, J.; Meng, S.; Niu, J.; Lu, H. Electronic structures and optical properties of monoclinic ZrO_2 studied by first-principles local density approximation + U approach. *J. Adv. Ceram.* **2017**, *6*, 43–49. https://doi.org/10.1007/s40145-016-0216-y.
16. Laudadio, E.; Stipa, P.; Pierantoni, L.; Mencarelli, D. Phase Properties of Different HfO_2 Polymorphs: A DFT-Based Study. *Crystals* **2022**, *12*. https://doi.org/10.3390/cryst12010090.
17. Low, J.J.; Paulson, N.H.; D'Mello, M.; Stan, M. Thermodynamics of monoclinic and tetragonal hafnium dioxide (HfO_2) at ambient pressure. *Calphad* **2021**, *72*, 102210. https://doi.org/10.1016/j.calphad.2020.102210.
18. Rivas-Silva, J.F.; Flores-Riveros, A.; Durand-Niconoff, J.S.; Aquino, N. Ab initio analysis of some fluoride and oxide structures doped with Pr and Yb. *Int. J. Quantum Chem.* **2004**, *97*, 815–825. https://doi.org/10.1002/qua.10779, https://doi.org/10.1002/qua.10779.
19. Smith, D.K.; Newkirk, W. The crystal structure of baddeleyite (monoclinic ZrO_2) and its relation to the polymorphism of ZrO_2. *Acta Cryst.* **1965**, *18*, 983–991. https://doi.org/10.1107/S0365110X65002402.

20. Howard, C.J.; Hill, R.J.; Reichert, B.E. Structures of ZrO_2 polymorphs at room temperature by high-resolution neutron powder diffraction. *Acta Crystallogr. B* **1988**, *44*, 116–120. https://doi.org/10.1107/S0108768187010279.

21. French, R.H.; Glass, S.J.; Ohuchi, F.S.; Xu, Y.N.; Ching, W.Y. Experimental and theoretical determination of the electronic structure and optical properties of three phases of ZrO_2. *Phys. Rev. B* **1994**, *49*, 5133–5142. https://doi.org/10.1103/PhysRevB.49.5133.

22. Lucovsky, G.; Fulton, C.C.; Zhang, Y.; Zou, Y.; Luning, J.; Edge, L.F.; Whitten, J.L.; Nemanich, R.J.; Ade, H.; Schlom, D.G.; et al. Conduction band-edge States associated with the removal of d-state degeneracies by the Jahn-Teller effect. *IEEE Trans. Device Mater. Reliab.* **2005**, *5*, 65–83. https://doi.org/10.1109/TDMR.2005.845804.

23. Balog, M.; Schieber, M.; Michman, M.; Patai, S. Chemical vapor deposition and characterization of HfO_2 films from organo-hafnium compounds. *Thin Solid Films* **1977**, *41*, 247–259. https://doi.org/10.1016/0040-6090(77)90312-1.

24. Pathak, S.; Das, P.; Das, T.; Mandal, G.; Joseph, B.; Sahu, M.; Kaushik, S.D.; Siruguri, V. Crystal structure of monoclinic hafnia (HfO_2) revisited with synchrotron X-ray, neutron diffraction and first-principles calculations. *Acta Crystallogr. C* **2020**, *76*, 1034–1042. https://doi.org/10.1107/S2053229620013960.

25. Legein, C.; Fayon, F.; Martineau, C.; Body, M.; Buzaré, J.Y.; Massiot, D.; Durand, E.; Tressaud, A.; Demourgues, A.; Péron, O.; et al. 19F High Magnetic Field NMR Study of β-ZrF_4 and CeF_4: From Spectra Reconstruction to Correlation between Fluorine Sites and 19F Isotropic Chemical Shifts. *Inorg. Chem.* **2006**, *45*, 10636–10641. https://doi.org/10.1021/ic061339a.

26. Benner, G.; Müller, B.G. Zur Kenntnis binärer Fluoride des ZrF_4-Typs: HfF_4 und ThF_4. *Z. anorg. allg. Chem.* **1990**, *588*, 33–42. https://doi.org/10.1002/zaac.19905880105.

27. Maimaitiyili, T.; Steuwer, A.; Blomqvist, J.; Bjerkén, C.; Blackmur, M.S.; Zanellato, O.; Andrieux, J.; Ribeiro, F. Observation of the δ to ϵ Zr-hydride transition by in-situ synchrotron X-ray diffraction. *Cryst. Res. Technol.* **2016**, *51*, 663–670. https://doi.org/10.1002/crat.201600234.

28. Romans, P.A.; Paasche, O.G.; Kato, H. The transformation temperature of hafnium. *J. Less-Common Met.* **1965**, *8*, 213–215. https://doi.org/10.1016/0022-5088(65)90048-2.

29. Block, S.; Da Jornada, J.A.H.; Piermarini, G.J. Pressure-Temperature Phase Diagram of Zirconia. *J. Am. Ceram. Soc.* **1985**, *68*, 497–499. https://doi.org/10.1111/j.1151-2916.1985.tb15817.x.

30. Al-Khatatbeh, Y.; Lee, K.K.M.; Kiefer, B. Phase diagram up to 105 GPa and mechanical strength of HfO_2. *Phys. Rev. B* **2010**, *82*, 144106. https://doi.org/10.1103/PhysRevB.82.144106.

31. McDonald, R.A.; Sinke, G.C.; Stull, D.R. High Temperature Enthalpy, Heat Capacity, Heat of Fusion, and Melting Point of Zirconium Tetrafluoride. *J. Chem. Eng. Data* **1962**, *7*, 83. https://doi.org/10.1021/je60012a026.

32. Sicius, H. Titangruppe: Elemente der vierten Nebengruppe. In *Handbuch der chemischen Elemente*; Sicius, H., Ed.; Springer Berlin Heidelberg: Berlin, Heidelberg, 2021; pp. 483–529. https://doi.org/10.1007/978-3-662-55939-0{_}9.

33. Goldstein, M.; Hughes, R.J.; Unsworth, W.D. Vibrational spectra of some heavy metal teftafluorides in the solid state. *Spectrochim. Acta A* **1975**, *31*, 621–624. https://doi.org/10.1016/0584-8539(75)80055-9.

34. Quintard, P.E.; Barbéris, P.; Mirgorodsky, A.P.; Merle-Méjean, T. Comparative Lattice-Dynamical Study of the Raman Spectra of Monoclinic and Tetragonal Phases of Zirconia and Hafnia. *J. Am. Ceram. Soc.* **2002**, *85*, 1745–1749. https://doi.org/10.1111/j.1151-2916.2002.tb00346.x.

35. Neese, F. Software update: The ORCA program system—Version 5.0. *WIREs Comput Mol Sci.* **2022**, *12*, e1606. https://doi.org/10.1002/wcms.1606, https://doi.org/10.1002/wcms.1606.

36. Weigend, F.; Ahlrichs, R. Balanced basis sets of split valence, triple zeta valence and quadruple zeta valence quality for H to Rn: Design and assessment of accuracy. *Phys. Chem. Chem. Phys.* **2005**, *7*, 3297–3305. https://doi.org/10.1039/B508541A.

37. Andrae, D.; Häußermann, U.; Dolg, M.; Stoll, H.; Preuß, H. Energy-adjusted ab initio pseudopotentials for the second and third row transition elements. *Theoret. Chim. Acta* **1990**, *77*, 123–141. https://doi.org/10.1007/BF01114537.

38. van Wüllen, C. Molecular density functional calculations in the regular relativistic approximation: Method, application to coinage metal diatomics, hydrides, fluorides and chlorides, and comparison with first-order relativistic calculations. *J. Chem. Phys.* **1998**, *109*, 392–399. doi: 10.1063/1.476576, https://doi.org/10.1063/1.476576.

39. Pantazis, D.A.; Chen, X.Y.; Landis, C.R.; Neese, F. All-Electron Scalar Relativistic Basis Sets for Third-Row Transition Metal Atoms. *J. Chem. Theory Comput.* **2008**, *4*, 908–919. doi: 10.1021/ct800047t, https://doi.org/10.1021/ct800047t.